

Induction of a Müller glial-specific protective pathway safeguards the retina from diabetes induced damage

Cheng-Hui Lin¹, Man-Ru Wu¹, Bogdan Tanasa¹, Praveen Prakhar¹, Boxiong Deng¹, Alexander E. Davis¹, Liang Li¹, Alexander Xia¹, Yang Shan², Patrice E. Fort², Sui Wang^{1*}

Supplementary information

- 1. Figure S1 to S11 with figure legends**
- 2. Supplementary Method and Materials**
- 3. Supplementary references**
- 4. Supplementary Table S1**
- 5. Supplementary Table S2 (excel file)**

Figure S1

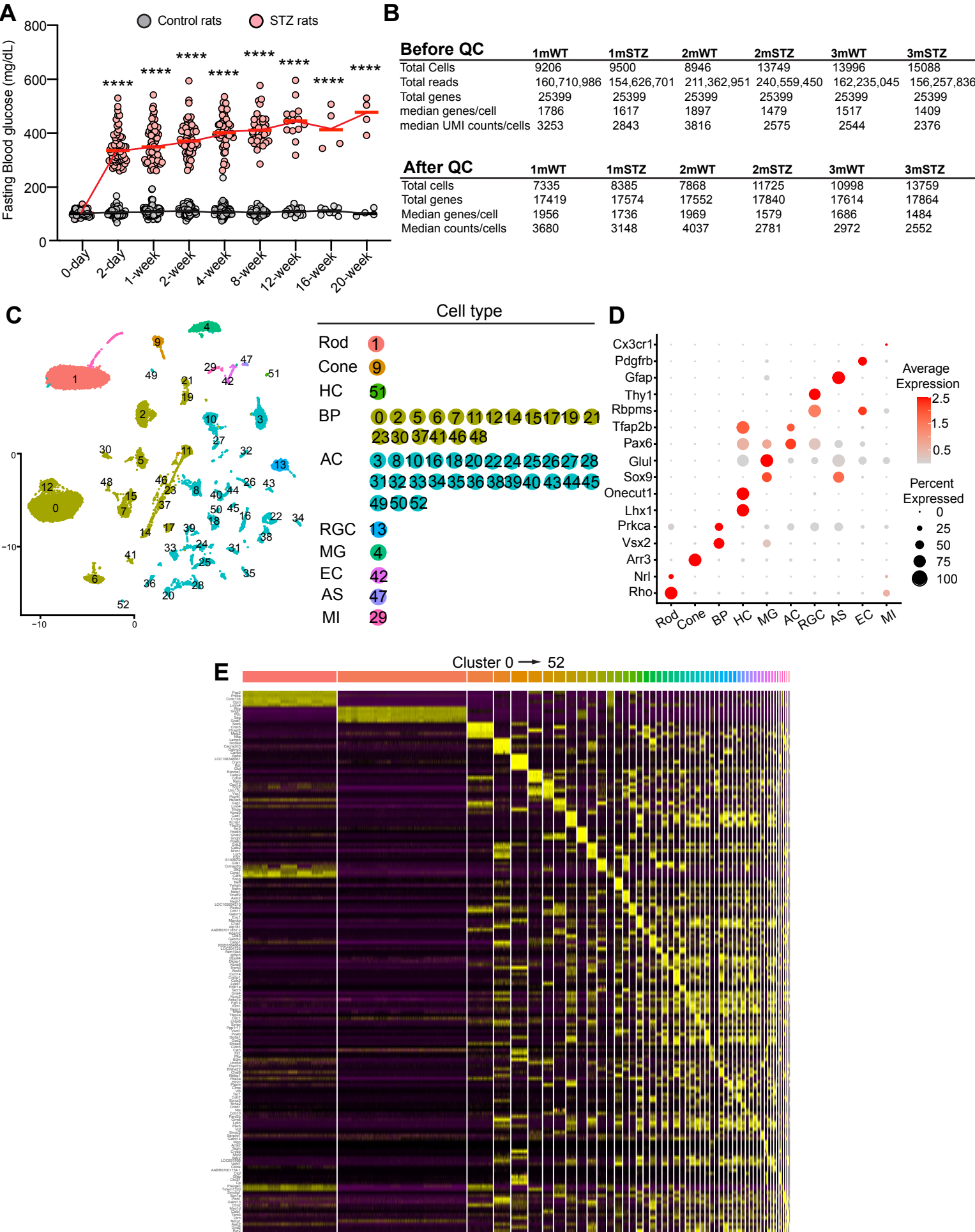


Figure S1. The quality control analyses of scRNA-seq data (related to Figure 1)

(A) Fasting blood glucose levels in male rats were monitored at 2 days, 1, 2, 4, 8, 12, 16, and 20 weeks post citrate buffer (control rats) or STZ (STZ rats) injection. Mean \pm SD. Unpaired t-test with Welch's correction (two-tailed). **** P < 0.0001. N numbers are indicated in the charts. **(B)** Summary of quality control metrics for each sample. **(C)** The relationship between cluster number and cell type. **(D)** Markers employed for the identification of major retinal cell types. **(E)** The top 5 differentially expressed genes for each cluster.

Figure S2

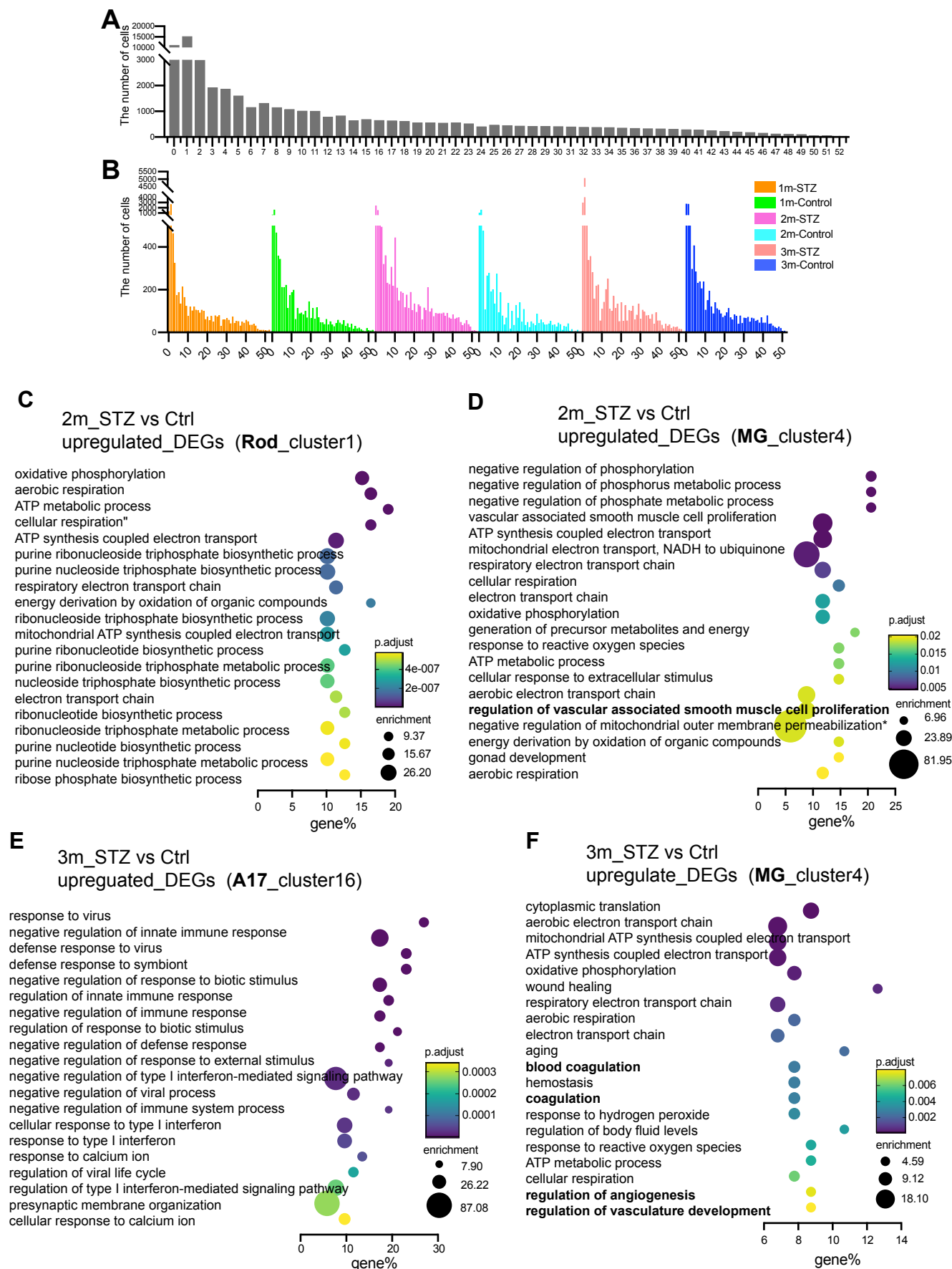


Figure S2. The number of cells captured in each cluster, and the enriched Gene Ontology (GO) terms for rod, Müller glial cells, and A17 amacrine cells at 2- or 3-month post STZ injection (related Figure 1 and 2).

(A-B) The quantity of retinal cells in each cluster post quality control is depicted, illustrating the total number of cells per cluster (A) and per cluster per condition (B). **(C-D)** The top 20 enriched GO terms for upregulated DEGs in rod (cluster 1, C) or Müller glial cells (cluster 4, D) at 2 months after STZ injection. **(E-F)** The top 20 enriched GO terms for upregulated DEGs in A17 amacrine cells (cluster 16, E) or Müller glial cells (cluster 4, F) at 3 months after STZ injection.

Figure S3

Gene	Function	Role	Supplementary References
Stat3	anti- or proinflammatory	Context-dependent	6-8
Cebpd	anti-apoptosis or pro-migration	Context-dependent	9, 10
Chka	oncogene	Negligent	11
Plat	activate microglia (act as a cytokine)	Negligent	12
Ctsc	pro-inflammation	Negligent	13
Slc3a2	oncogene	Negligent	14, 15
Ano6	oncogene	Negligent	16
Vav3	anti-survival	Negligent	17
Ptpn	oncogene	Negligent	18
Plin2	pro-inflammation	Negligent	19
Rnf19b	anti-inflammation	Protective	20
Lcn2	Neuroprotective	Protective	21
Dclk1	pro-survival	Protective	22, 23
Scg2	anti-angiogenesis	Protective	24, 25
Enox1	anti-apoptosis, anti-angiogenesis	Protective	26, 27
Slc7a11	neuroprotective, anti oxidative stress	Protective	28
Ifrd1	anti-inflammation, anti-apoptosis	Protective	29
Qsox1	anti-inflammation	Protective	30
Zfp36	anti-inflammation	Protective	31
Cyp26a1	anti-apoptosis	Protective	32-34
Mt3	anti-oxidative stress	Protective	35, 36
Mt1	anti-oxidative stress	Protective	37
Akap12	anti-oxidative stress, anti-inflammation, anti-angiogenesis	Protective	38, 39
AABR07040864.1	anti-apoptosis	Protective	40
Cited2	anti-inflammation	Protective	41
Mt2A	anti-oxidant, anti-apoptosis, detoxification, anti-proliferation anti-inflammation	Protective	42
Mt1m	anti-proliferation	Protective	43
Slc14a1	neuroprotective	Protective	44
Cp	neuroprotective, anti-oxidative stress	Protective	45
Rnd3	anti-proliferation	Protective	46
Dusp6	neuroprotective	Protective	47
Timp1	anti-inflammation	Protective	48, 49
Gdpd2	Unknown	Unknown	
Ac128848.1	Unknown	Unknown	
Sorcs1	Unknown	Unknown	
Col5a3	Unknown	Unknown	

Figure S3. The predicted roles of the DEGs that are temporarily upregulated at 1 month (up-down DEGs, 1m_STZ vs 1m_Ctrl) in Müller glial cells based on the literature (related to Figure 2)

The gene name, function, predicted roles and references are listed.

Figure S4

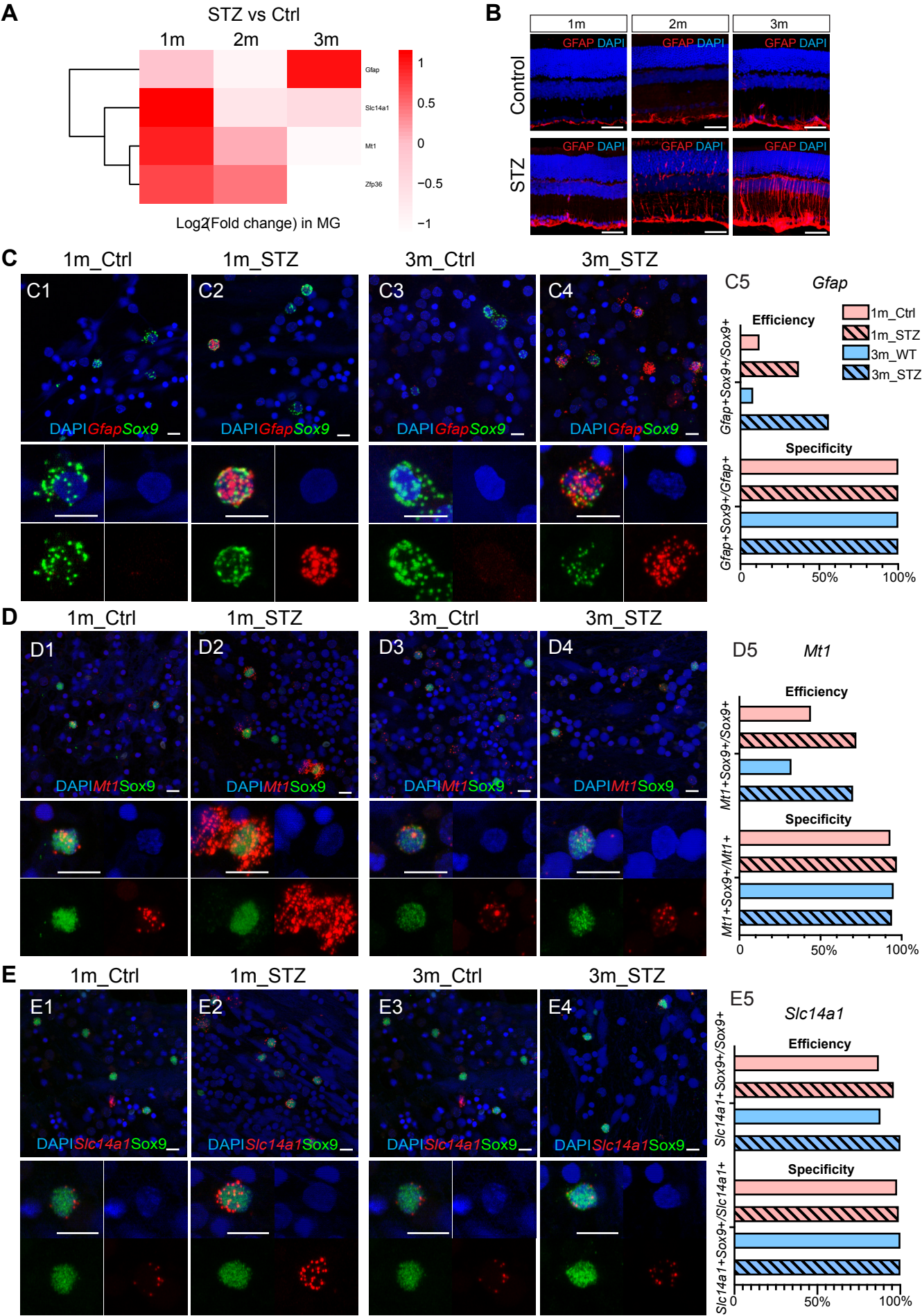


Figure S4. The expression of *Gfap* and candidate protective genes in Müller glial cells at 1 to 3 months post citrate buffer or STZ injection (related to Figure 2)

(A) Heatmap illustrating the \log_2 (fold changes) of *Gfap*, *Mt1*, *Slc14a1* and *Zfp36* in Müller glial cells (MG) at 1, 2, or 3 months after citrate buffer or STZ injection. **(B)** The expression of GFAP protein in rat retinas. 1m, 2m or 3m: 1, 2 or 3 months after injection. Control: with citrate buffer injection. STZ: with STZ injection. **(C)** *Gfap* expression (red signal). Sox9 smFISH signals (green) indicate Müller glial cells (MG). The percentage of MG expressing *Gfap* (efficiency) and the percentage of *Gfap*⁺ cells that are MG (specificity) are shown in A5. **(D)** *Mt1* expression (red signal). Sox9 antibody staining signals (green) indicate Müller glial cells (MG). The percentage of MG expressing *Mt1* (efficiency) and the percentage of *Mt1*⁺ cells that are MG (specificity) are shown in A5. **(E)** *Slc14a1* expression (red signal). Sox9 antibody staining signals (green) indicate Müller glial cells (MG). The percentage of MG expressing *Slc14a1* (efficiency) and the percentage of *Slc14a1*⁺ cells that are MG (specificity) are shown in A5.

Figure S5

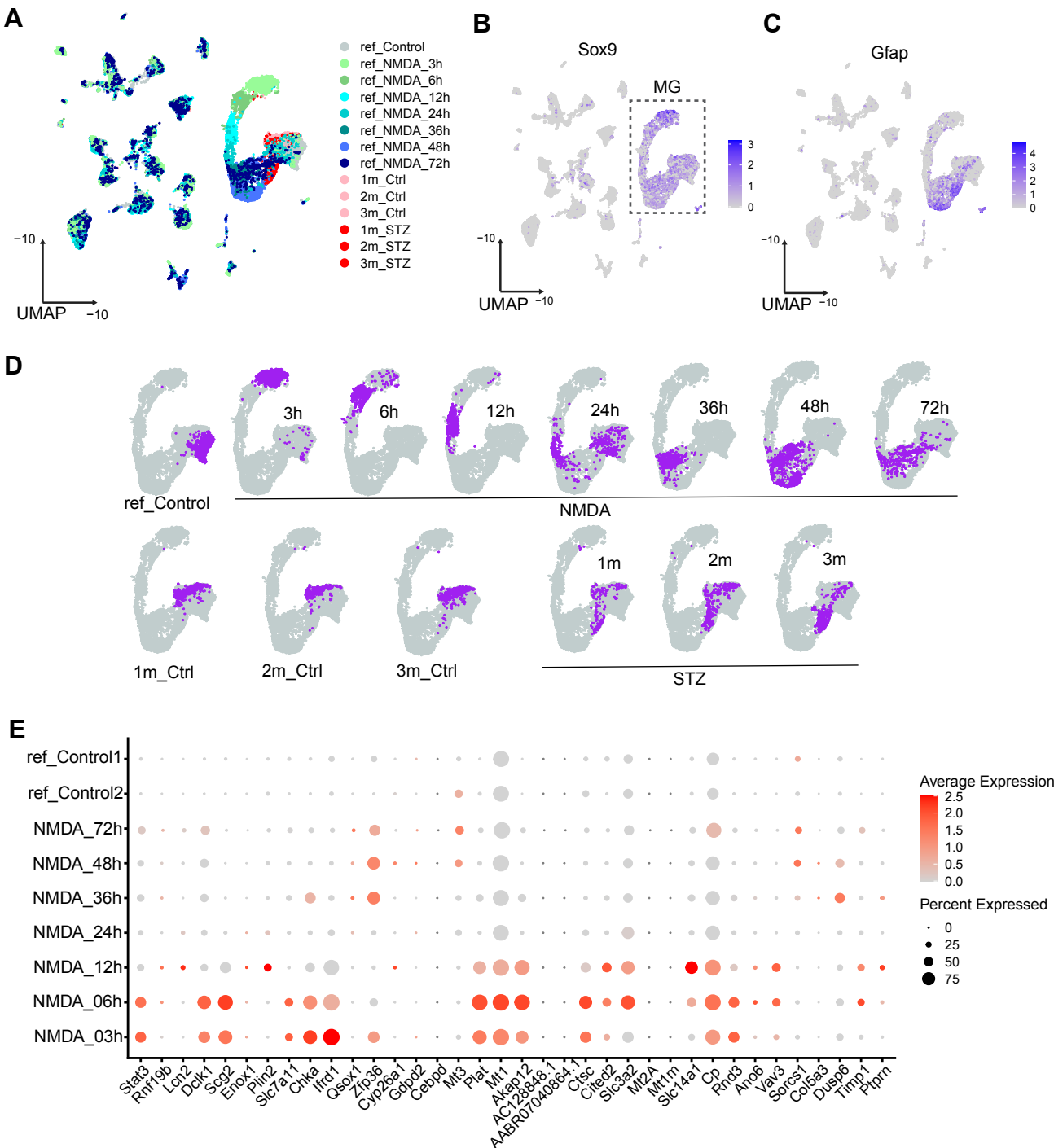


Figure S5. A comparison between Müller glial cells (MG) from rat diabetic retinas and those from an acute injury mouse model, revealing partially overlapping transcriptional profiles.

(A) UMAP plot illustrating diabetic rat MG (query) and mouse MG subjected to NMDA treatment (reference). **(B)** UMAP plot illustrating the expression of *Sox9*, with the MG cluster outlined by a dotted line box. **(C)** UMAP plot illustrating the expression of *Gfap*, indicating gliosis in MG. **(D)** UMAP plots illustrating MG profiles under different conditions. Wild type control mouse MG are depicted on the top, while control or STZ rat MG are illustrated at the bottom. **(E)** Dotplot showing the expression of DEGs that are temporarily upregulated at 1 month (1m up-down DEGs, 1m_STZ vs 1m_Ctrl) in NMDA treated mouse MG at various time points post NMDA injection.

Figure S6

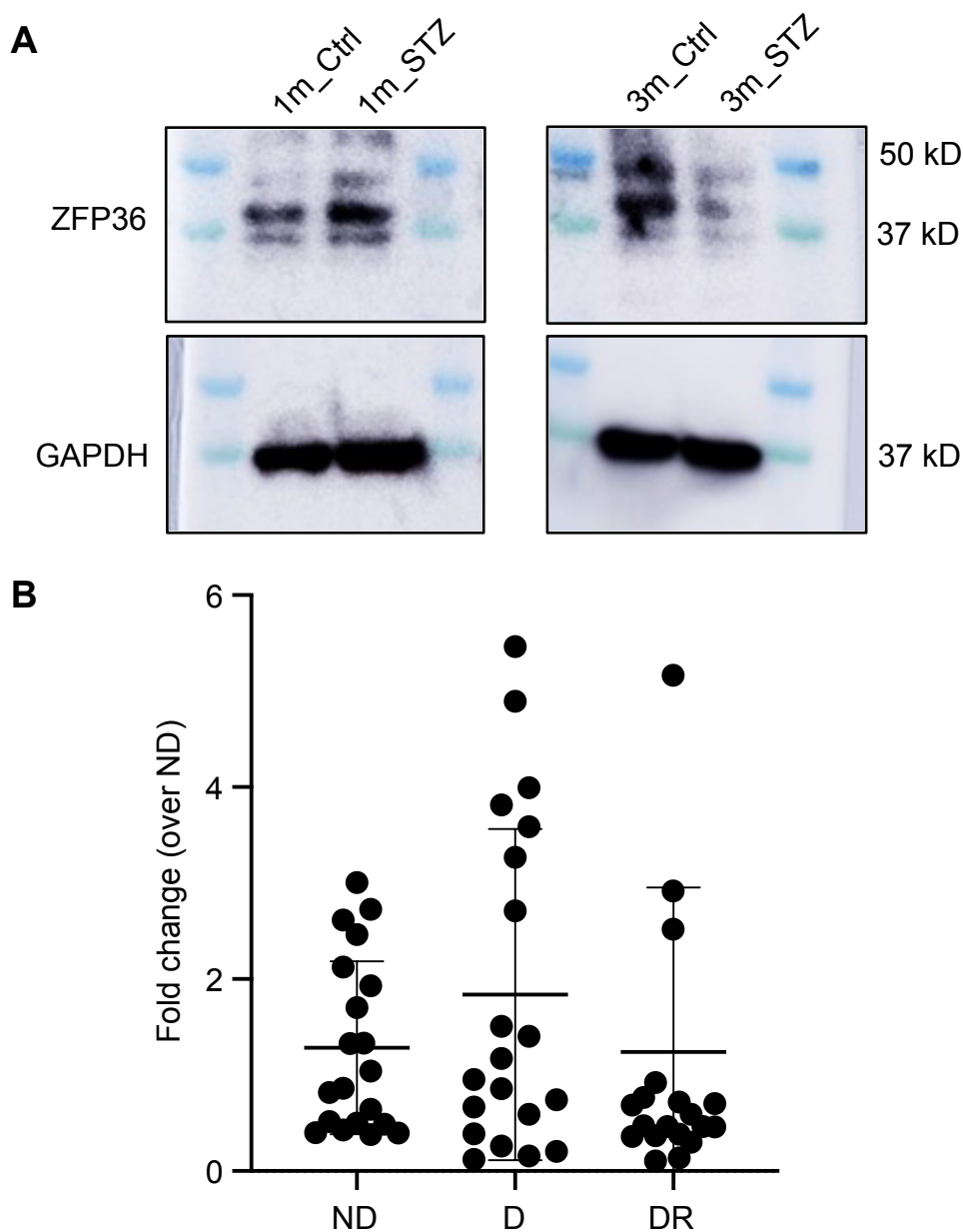


Figure S6. Zfp36 is transiently upregulated in diabetic retinas (related to Figure 3).

(A) ZFP36 and GAPDH were detected by western blotting in rat retinas at 1 month or 3 months post STZ injection. **(B)** The expression of *Zfp36* in human retinas was detected by qPCR. ND: healthy control; D: diabetic control without DR; DR: human retina samples with DR.

Figure S7

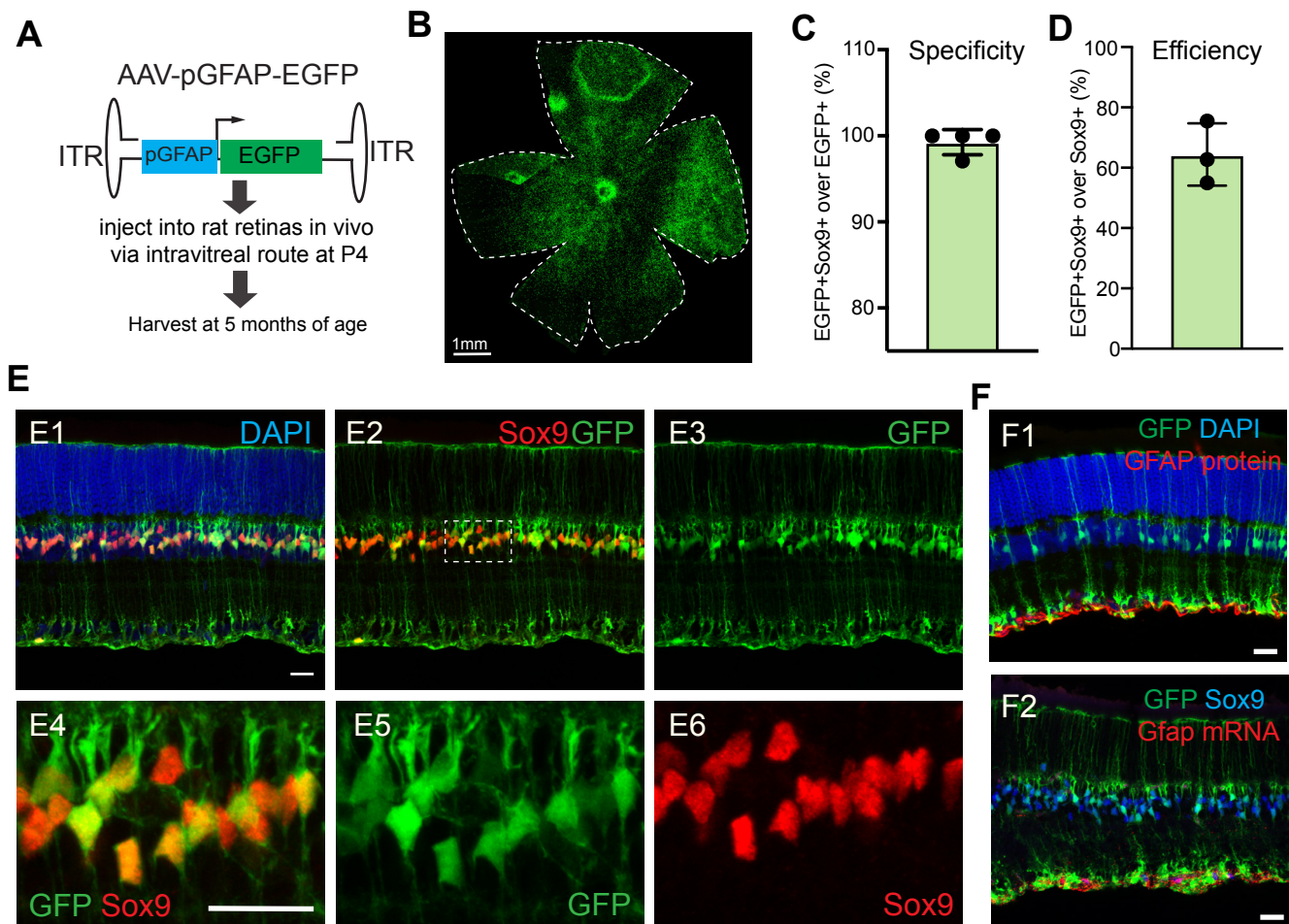


Figure S7. The efficiency and specificity of AAV7m8-pGFAP-EGFP (related to Figure 4 and 5)

(A) The AAV-pGFAP-EGFP construct and the experimental schematic design. **(B)** A representative image showing the transduction efficiency of AAV7m8-pGFAP-EGFP. Scale bar: 1mm. **(C-D)** The specificity (C) and efficiency (D) of AAV7m8-pGFAP-EGFP in labeling rat Müller glial cells. **(E)** Representative images showing the specificity and efficiency of AAV7m8-pGFAP-EGFP. Red: Sox9 antibody staining signals (Müller glial cell marker). Scale bar: 20um. **(F)** The *Gfap* mRNA and protein are not induced upon injection of AAV7m8-pGFAP-EGFP into the retina. Scale bar: 20um.

Figure S8

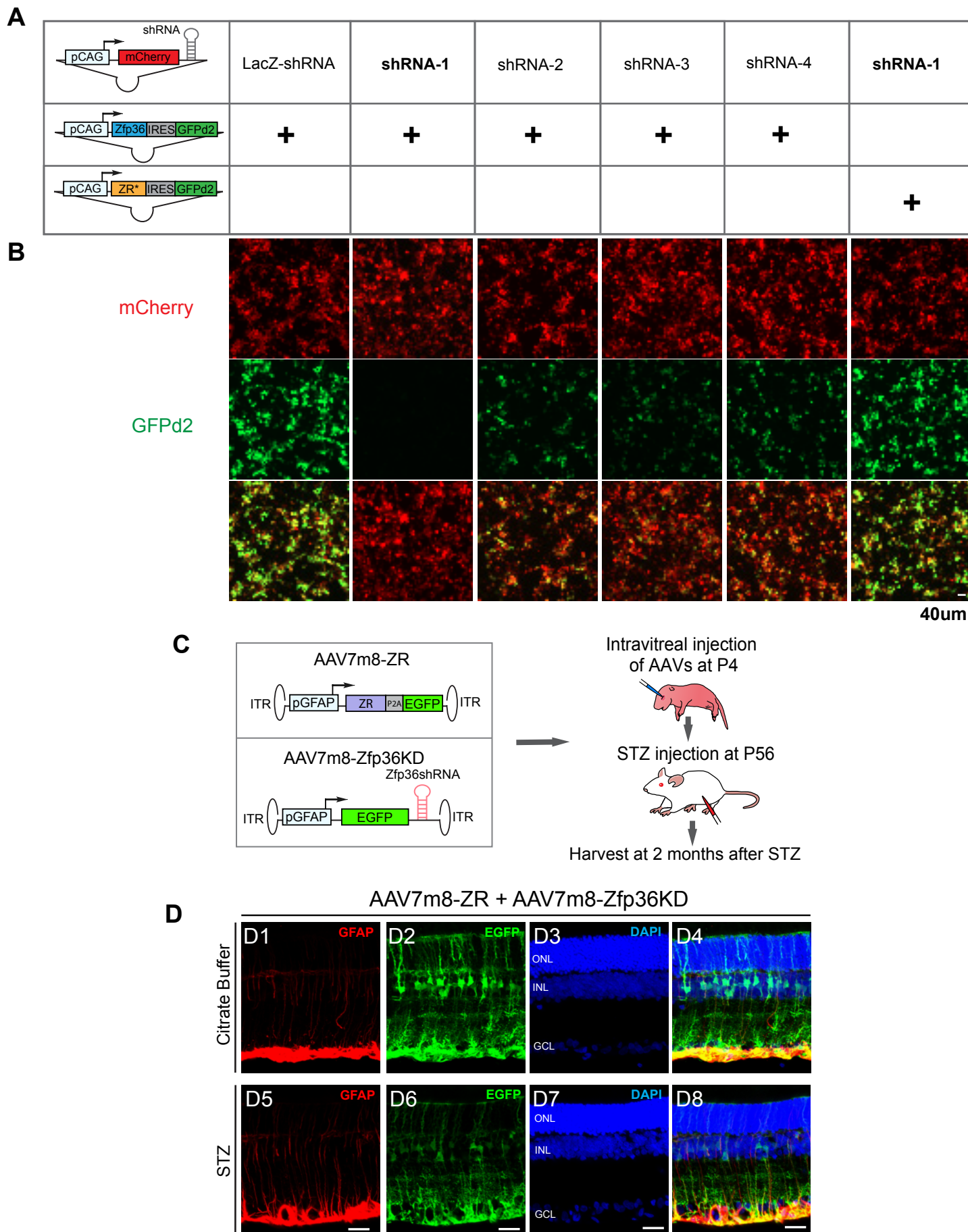


Figure S8. The knocking down efficiency of Zfp36-shRNA and its rescue by AAV7m8-ZR (related to Figure 4)

(A-B) The experimental design schematic (A). shRNA-76 can efficiently knock down Zfp36 expression in HEK 293T cells in vitro (B). The ZR construct rescues this effect. GFPd2: destabilized form of GFP. **(C-D)** The experimental design schematic (C). The representative images showing retinas received AAV7m8-ZR and AAV7m8-Zfp36KD with citrate buffer or STZ injection (D). Red: GFAP staining. Scale bar: 20um.

Figure S9

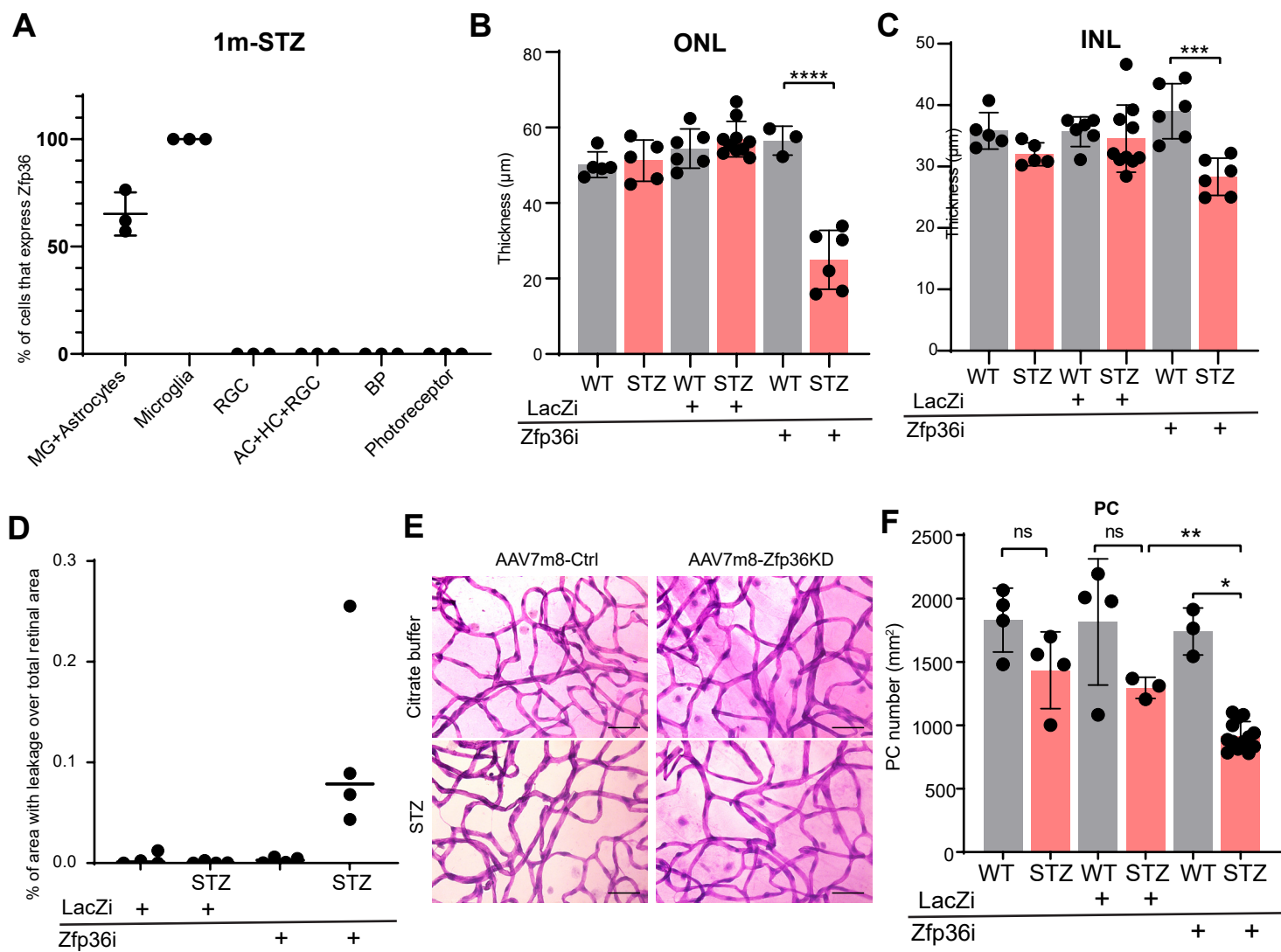


Figure S9. The expression of *Zfp36* in STZ retinas, and retinal phenotypes induced by *Zfp36* KD (related to Figure 3 and 4)

(A) Percentage of indicated cell types expressing *Zfp36* in STZ rat retinas at 1 month post STZ. **(B-C)**. Quantification of retinal ONL (Outer nuclear layer, B) and INL (Inner nuclear layer, C) thickness in control and STZ retinas. Mean \pm SD. Unpaired t-test with Welch's correction (two-tailed). *** $P < 0.001$, N numbers indicated in the charts. LacZi: rats received AAV7m8-Ctrl. *Zfp36*i: rats received AAV7m8-*Zfp36*KD. **(D)** The percentage of area with leakage over total retinal area at 2 months post STZ. **(E)** The Representative images of elastase digestion. Scale bar: 50um. **(F)** Quantification of pericyte numbers in retinas received AAV7m8-ZR or AAV7m8-*Zfp36*KD with citrate buffer or STZ injection. Mean \pm SD. Unpaired t-test with Welch's correction (two-tailed). * $P < 0.05$, ** $P < 0.01$, ns $P \geq 0.05$. N numbers indicated in the charts.

Figure S10

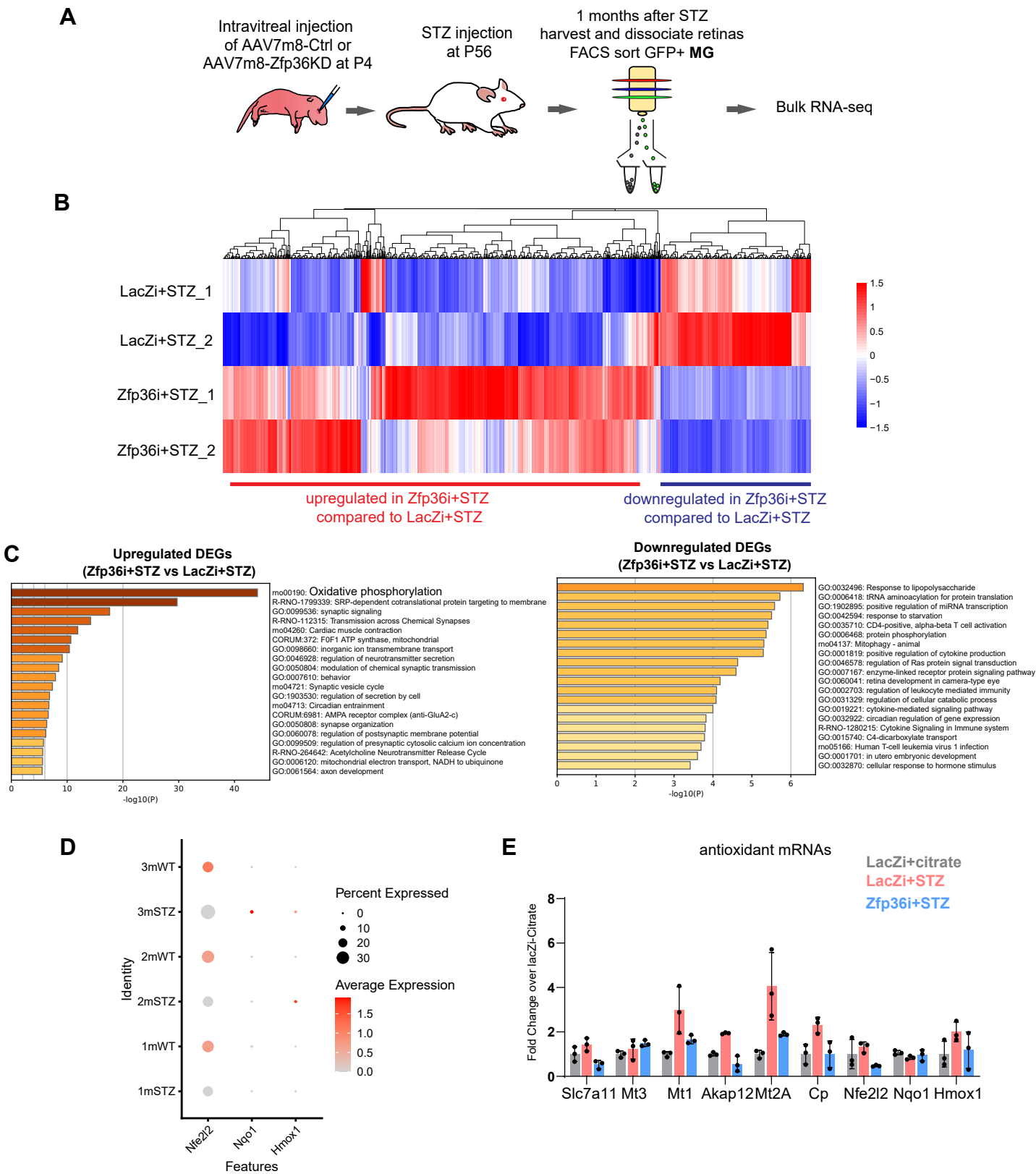


Figure S10. Potential molecular events downstream of Zfp36KD (related Figure 4 and Discussion)

(A) The experimental design. **(B)**. Heatmap showing DEGs comparing Zfp36i+STZ vs LacZi+STZ Müller glial cells. Blue: downregulated genes; Red: upregulated genes. **(C)** GO enrichment analyses of upregulated or downregulated DEGs. **(D)** Dotplot showing the expression of *Nfe2l2* (encoding Nrf2) and Nrf responsive genes *Nqo1* and *Hmox1* in WT or STZ retinas at 1, 2 or 3 months post STZ. **(E)** qPCR showing the expression levels of antioxidant genes in LacZi+citrate, LacZi+STZ, and Zfp36i+STZ Müller glial cells.

Figure S11

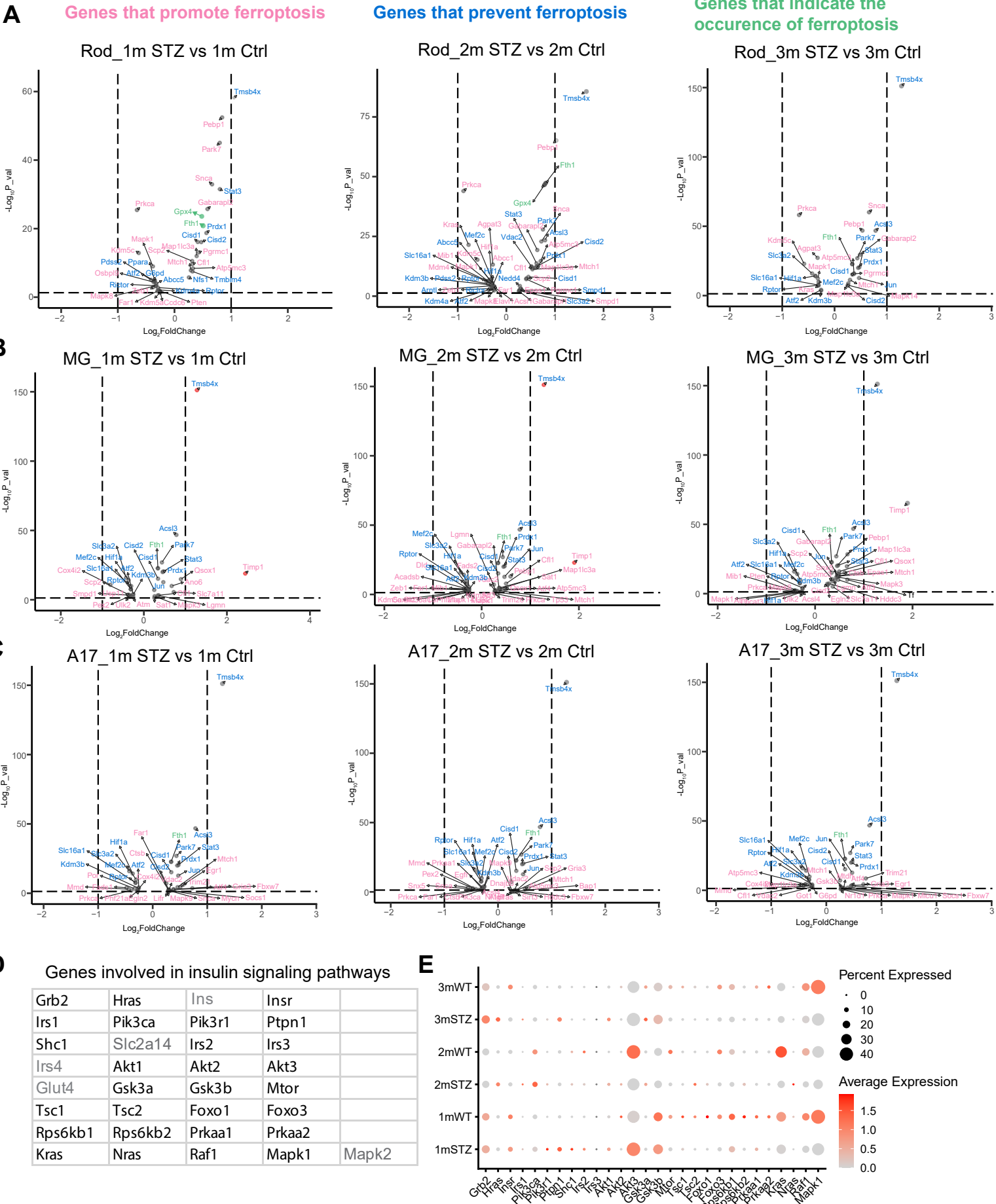


Figure S11. The expression of ferroptosis-related genes and insulin signaling related genes in diabetic retinas (related to Figure 1)

(A-C). Volcano plot showing the expression of ferroptosis-related genes in rod, Müller glial cells (MG) and A17 cells at 1, 2 or 3 months post STZ injection. Genes that promote ferroptosis are labeled pink. Genes that prevent ferroptosis are labeled blue. Genes that indicate the occurrence of ferroptosis are labeled green. Dotted lines: $|\log_2(\text{FoldChange})| > 1$. **(D)** Known genes involved in insulin signaling pathways. Gray: not detected in our scRNA-seq dataset (*Ins*, *Slc2a14*, *Irs4*, *Glut4* and *Mapk2*). **(E)** Dotplot showing the expression levels of insulin signaling related genes in WT or STZ retinas at 1, 2 or 3 months post STZ.

Supplementary Method and Materials

Induction of Diabetes

STZ (Sigma #0130) injection was carried out in accordance with the established protocol(1) with a dosage of 65mg/kg rat. Rats exhibiting consistently elevated fasting glucose levels exceeding 250mg/dl at 2, 7 days, 2 weeks, 1, 2, or 3 months post injection were included. Insulin was intentionally omitted to mitigate confounding factors.

Plasmid construction

The AAV-pGFAP-EGFP plasmid was used as the backbone(2). The shRNA cassettes were crafted in accordance with established methodologies(3). The AAV-Ctrl and AAV-Zfp36-KD plasmids were generated by integrating the LacZ-shRNA or Zfp36-shRNA cassette (shRNA-76, Figure S8) into the backbone(2). The AAV-pGFAP-ZR-p2A-EGFP plasmid was constructed by inserting a codon-optimized rat Zfp36 ORF, designed to be impervious to Zfp36-shRNA recognition into the backbone. The AAV-pGFAP-Zfp36-p2A-EGFP plasmid was created by introducing the wildtype *Zfp36* ORF into the backbone. Details of sequences are outlined in Table S1.

Adeno-Associated Virus (AAV) Production and Delivery

Recombinant AAV7m8 viruses were produced and injected intravitreally following a prior publication(2). Approximately 1.5 μ l of AAV7m8 ($\sim 10^{12}$ gc/ml) was injected per eye.

Histology and Immunohistochemistry

Cryosections and wholemounts of rat retinas were prepared and stained following published protocols(2). Primary antibodies utilized include chicken anti-GFP (Abcam, ab13970), rabbit anti-Sox9 (Abcam, ab185966,, chicken anti-GFAP (Fisher scientific, NBP105198,, rabbit anti-Pax6 (ThermoFisher Scientific, 42-6600), sheep anti Chx10(Vsx2) (Exalpha Biologicals, X1179P), Guinea pig anti RBPMS (PhosphoSolutions, 1832-RBPMS), goat anti Iba1 (Abcam, ab5076),

AlexaFluor 647-conjugated IB4 (ThermoFisher, I32450), and Rabbit anti-Desmin (Abcam, ab15200).

mRNA FISH

Rat retinal cells were prepared following established procedures(4). Probes were purchased from ACDBio, and FISH was conducted according to commercial protocols.

Western blot

Western blot were performed following established procedure(5). The Zfp36 signals were captured using the Amersham ImageQuant 600 (Cytiva) system. After imaging, Zfp36 signals were stripped from the membrane (ThermoFisher, 21059), and rabbit anti-GAPDH (Abcam, ab9485) was applied and imaged.

Retina Vessel Permeability Assay

NHS-Biotin (Thermo Fisher Scientific; 21335) was injected into the left ventricle of anesthetized rats at the dosage of 0.4 mg/g body weight. Rats exhibiting a continuous, steady heartbeat for 7 minutes were included in the study. After 15 minutes of tracer circulation, eyeballs were enucleated and fixed in 4% paraformaldehyde. AlexaFluor555-conjugated Streptavidin (ThermoFisher, S21381) was used for NHS-Biotin detection.

Imaging and analysis

Retinal images were captured using Zeiss LSM880 or Olympus FV3000 confocal microscopes. The images presented in Figures 3, 4, and 5 represent maximum projections of 5-10 μ m tissue sections, and their quantification was performed using Fiji software.

Supplementary References

1. Furman, B. L. (2015) Streptozotocin-Induced Diabetic Models in Mice and Rats. *Curr Protoc Pharmacol.* **70**, 5.47.1-5.47.20
2. Lin, C.-H., Sun, Y., Chan, C. S. Y., Wu, M.-R., Gu, L., Davis, A. E., Gu, B., Zhang, W., Tanasa, B., Zhong, L. R., Emerson, M. M., Chen, L., Ding, J. B., and Wang, S. (2022) Identification of cis-regulatory modules for adeno-associated virus-based cell-type-specific targeting in the retina and brain. *Journal of Biological Chemistry.* 10.1016/j.jbc.2022.101674
3. Wang, S., Sengel, C., Emerson, M. M., and Cepko, C. L. (2014) A gene regulatory network controls the binary fate decision of rod and bipolar cells in the vertebrate retina. *Dev Cell.* **30**, 513–527
4. Trimarchi, J. M., Harpavat, S., Billings, N. A., and Cepko, C. L. (2008) Thyroid hormone components are expressed in three sequential waves during development of the chick retina. *BMC Dev. Biol.* **8**, 101
5. Li, L., Sun, Y., Davis, A. E., Shah, S. H., Hamed, L. K., Wu, M.-R., Lin, C.-H., Ding, J. B., and Wang, S. (2023) Mettl14-mediated m6A modification ensures the cell-cycle progression of late-born retinal progenitor cells. *Cell Rep.* **42**, 112596
6. Herrmann, J. E. *et al.* STAT3 is a Critical Regulator of Astrogliosis and Scar Formation after Spinal Cord Injury. *J Neurosci* **28**, 7231–7243 (2008).
7. Przanowski, P. *et al.* The signal transducers Stat1 and Stat3 and their novel target Jmjd3 drive the expression of inflammatory genes in microglia. *J Mol Med (Berl)* **92**, 239–254 (2014).
8. Kim, J. A. *et al.* Inhibitory effect of a 2,4-bis(4-hydroxyphenyl)-2-butenal diacetate on neuro-inflammatory reactions via inhibition of STAT1 and STAT3 activation in cultured astrocytes and microglial BV-2 cells. *Neuropharmacology* **79**, 476–487 (2014).
9. Ko, C.-Y., Chang, W.-C. & Wang, J.-M. Biological roles of CCAAT/Enhancer-binding protein delta during inflammation. *Journal of Biomedical Science* **22**, 6 (2015).
10. Wang, S.-M. *et al.* Increase of zinc finger protein 179 in response to CCAAT/enhancer binding protein delta conferring an antiapoptotic effect in astrocytes of Alzheimer's disease. *Mol Neurobiol* **51**, 370–382 (2015).
11. Chen, X. *et al.* Molecular structure and differential function of choline kinases CHK α and CHK β in musculoskeletal system and cancer. *Cytokine & Growth Factor Reviews* **33**, 65–72 (2017).
12. Siao, C.-J., Fernandez, S. R. & Tsirka, S. E. Cell type-specific roles for tissue plasminogen activator released by neurons or microglia after excitotoxic injury. *J Neurosci* **23**, 3234–3242 (2003).
13. Zhao, X. *et al.* Cathepsin C aggravates neuroinflammation via promoting production of CCL2 and CXCL2 in glial cells and neurons in a cryogenic brain lesion. *Neurochem Int* **148**, 105107 (2021).
14. Anagnostakis, F., Kokkorakis, M., Markouli, M. & Piperi, C. Impact of Solute Carrier Transporters in Glioma Pathology: A Comprehensive Review. *Int J Mol Sci* **24**, 9393 (2023).
15. Feral, C. C. *et al.* CD98hc (SLC3A2) mediates integrin signaling. *Proc Natl Acad Sci U S A* **102**, 355–360 (2005).
16. Xuan, Z., Wang, Y. & Xie, J. ANO6 promotes cell proliferation and invasion in glioma through regulating the ERK signaling pathway. *Onco Targets Ther* **12**, 6721–6731 (2019).

17. Wegrzyn, D., Zokol, J. & Faissner, A. Vav3-Deficient Astrocytes Enhance the Dendritic Development of Hippocampal Neurons in an Indirect Co-culture System. *Front Cell Neurosci* **15**, 817277 (2022).
18. Li, P. *et al.* PTPRN Serves as a Prognostic Biomarker and Correlated with Immune Infiltrates in Low Grade Glioma. *Brain Sci* **12**, 763 (2022).
19. Zhang, S. *et al.* PLIN2 Mediates Neuroinflammation and Oxidative/Nitrosative Stress via Downregulating Phosphatidylethanolamine in the Rostral Ventrolateral Medulla of Stressed Hypertensive Rats. *J Inflamm Res* **14**, 6331–6348 (2021).
20. Wu, C. *et al.* NLRP11 attenuates Toll-like receptor signalling by targeting TRAF6 for degradation via the ubiquitin ligase RNF19A. *Nat Commun* **8**, 1977 (2017).
21. Gasterich, N. *et al.* Lipocalin 2 attenuates oligodendrocyte loss and immune cell infiltration in mouse models for multiple sclerosis. *Glia* **70**, 2188–2206 (2022).
22. Chandrakesan, P. *et al.* Dclk1, a tumor stem cell marker, regulates pro-survival signaling and self-renewal of intestinal tumor cells. *Molecular Cancer* **16**, 30 (2017).
23. Vreugdenhil, E. *et al.* Doublecortin-like, a microtubule-associated protein expressed in radial glia, is crucial for neuronal precursor division and radial process stability. *Eur J Neurosci* **25**, 635–648 (2007).
24. Fang, C. *et al.* Secretogranin II impairs tumor growth and angiogenesis by promoting degradation of hypoxia-inducible factor-1 α in colorectal cancer. *Mol Oncol* **15**, 3513–3526 (2021).
25. Steinfass, T. *et al.* Secretogranin II influences the assembly and function of MHC class I in melanoma. *Experimental Hematology & Oncology* **12**, 29 (2023).
26. Geng, L. *et al.* Indolyl-quinuclidinols inhibit ENOX activity and endothelial cell morphogenesis while enhancing radiation-mediated control of tumor vasculature. *FASEB J* **23**, 2986–2995 (2009).
27. Venkateswaran, A. *et al.* The NADH oxidase ENOX1, a critical mediator of endothelial cell radiosensitization, is crucial for vascular development. *Cancer Res* **74**, 38–43 (2014).
28. Shih, A. Y. *et al.* Cystine/glutamate exchange modulates glutathione supply for neuroprotection from oxidative stress and cell proliferation. *J Neurosci* **26**, 10514–10523 (2006).
29. Tummers, B. *et al.* The interferon-related developmental regulator 1 is used by human papillomavirus to suppress NF κ B activation. *Nat Commun* **6**, 6537 (2015).
30. Geng, Y., Xu, C., Wang, Y. & Zhang, L. Quiescin Sulfhydryl Oxidase 1 Regulates the Proliferation, Migration and Invasion of Human Glioblastoma Cells via PI3K/Akt Pathway. *Onco Targets Ther* **13**, 5721–5729 (2020).
31. Mukherjee, N. *et al.* Global target mRNA specification and regulation by the RNA-binding protein ZFP36. *Genome Biol.* **15**, R12 (2014).
32. Osanai, M. & Petkovich, M. Expression of the retinoic acid-metabolizing enzyme CYP26A1 limits programmed cell death. *Mol Pharmacol* **67**, 1808–1817 (2005).
33. Cao, D.-L., Ma, L.-J., Jiang, B.-C., Gu, Q. & Gao, Y.-J. Cytochrome P450 26A1 Contributes to the Maintenance of Neuropathic Pain. *Neurosci. Bull.* (2023) doi:10.1007/s12264-023-01101-1.
34. Retinoic acid signaling mediates peripheral cone photoreceptor survival in a mouse model of retina degeneration | eLife. <https://elifesciences.org/articles/76389>.
35. Koh, J.-Y. & Lee, S.-J. Metallothionein-3 as a multifunctional player in the control of cellular processes and diseases. *Mol Brain* **13**, 116 (2020).

36. Tsuruma, K. *et al.* Metallothionein-III deficiency exacerbates light-induced retinal degeneration. *Invest Ophthalmol Vis Sci* **53**, 7896–7903 (2012).
37. Dai, H., Wang, L., Li, L., Huang, Z. & Ye, L. Metallothionein 1: A New Spotlight on Inflammatory Diseases. *Frontiers in Immunology* **12**, (2021).
38. Takase, H. *et al.* Roles of A-kinase anchor protein 12 in astrocyte and oligodendrocyte precursor cell in postnatal corpus callosum. *Stem Cell Rev Rep* **17**, 1446–1455 (2021).
39. Li, H. Physiologic and pathophysiologic roles of AKAP12. *Sci Prog* **105**, 00368504221109212 (2022).
40. Yan, C. *et al.* Overexpression of ATG4a promotes autophagy and proliferation, and inhibits apoptosis in lens epithelial cells via the AMPK and Akt pathways. *Mol Med Rep* **22**, 1295–1302 (2020).
41. Pong Ng, H., Kim, G.-D., Ricky Chan, E., Dunwoodie, S. L. & Mahabeleshwar, G. H. CITED2 limits pathogenic inflammatory gene programs in myeloid cells. *FASEB J* **34**, 12100–12113 (2020).
42. Ling, X.-B. *et al.* Mammalian Metallothionein-2A and Oxidative Stress. *Int J Mol Sci* **17**, 1483 (2016).
43. Mao, J. *et al.* Metallothionein MT1M is a tumor suppressor of human hepatocellular carcinomas. *Carcinogenesis* **33**, 2568–2577 (2012).
44. Yang, B. *et al.* Extrarenal phenotypes of the UT-B knockout mouse. *Subcell Biochem* **73**, 153–164 (2014).
45. Santiago González, D. A., Cheli, V. T., Rosenblum, S. L., Denaroso, G. & Paez, P. M. Ceruloplasmin deletion in myelinating glial cells induces myelin disruption and oxidative stress in the central and peripheral nervous systems. *Redox Biol* **46**, 102118 (2021).
46. Pacary, E., Azzarelli, R. & Guillemot, F. Rnd3 coordinates early steps of cortical neurogenesis through actin dependent and independent mechanisms. *Nat Commun* **4**, 1635 (2013).
47. Huang, X. *et al.* Neuroprotective effect of dual specificity phosphatase 6 against glutamate-induced cytotoxicity in mouse hippocampal neurons. *Biomed Pharmacother* **91**, 385–392 (2017).
48. Moore, C. S. *et al.* Astrocytic Tissue Inhibitor of Metalloproteinase-1 (TIMP-1) Promotes Oligodendrocyte Differentiation and Enhances CNS Myelination. *J Neurosci* **31**, 6247–6254 (2011).
49. Sutter, P. A. *et al.* Astrocytic TIMP-1 regulates production of Anastellin, a novel inhibitor of oligodendrocyte differentiation and FTY720 responses. *bioRxiv* 2023.02.17.529003 (2023) doi:10.1101/2023.02.17.529003

Table S1. The primers and DNA sequences used in the study

Name	Sequence (5'-3')	Experiments
Zfp36-shRNA-1	TGGAGGCTTGCTGAAGGCgtgaTGCTGATCGACATAAGGCTCTCGTAGGTTTTGGCCACT GACTGACCTACGAGACTTATGTGATCAGGACACAAGGCCTGTTACTAGCACTCACATG GAACAAAT	shRNA with flanking sequences
ZR-p2A-EGFP	ATGGCCATTGCGGCCACCATGGATCTCTCTGCCATatatgaatctctcatgagcatGAGCCATGACCTGTCA CCCCACCACGGAGGAAGTGAAGTCCCTCCGAGGACTTTGGAACATAAACTCATCGGACTCCATCC CATCTGGGGTACCTCTCGCCTGACTGGCCGCTCCACTAGCCTGGTGGAGGGCCGAAGCTGCA GCTGGGTACCCCAACCCCTGGTTTCGACCCCTTGGCTCCCCGCCGGGCCCTGAGCTGTAC CCTCACCTACTTCGCCTACTGCAACTCCACCACCTCCTCTCGATACAAGACTGAGCTCTGTCCG ACCTACTCAGAGAGCGGGCGTTGTGCTATGGGGCCAAGTGCCAGTTTGCCACGGCCCGGGT GAACTGCGCCAAAGCCAATCGCCACCCCAAGTACAAAACGGAACTCTGCCACAAGTTCTACCTCCA GGGCCGCTGCCCTACGGCTCTCGATGCCACTTCATCCACAACCTACCGAGGACCTGGCTCTC CCTGGCCAGCCCATGTGCTCCGACAAAGCATCAGCTTCTCAGGCTTGCCCTCAGGCCGAGAA CCTCACCACACCTCCAGGCTTCTCTGGCCCTTCCCTGTCTCTTGTCTCTTTCCGCTTCCAGC TCCCCACCACCGCTCGGGGACCTTCCACTTTCCCTTCTGCTTCTCTGCTGCCCTGGGACCC CTGTGTCTCGAAGAGACCTACCCAGCCTGTTGTCCCTCCTGCCGAAGGTCTACTACCCCTAG CACCATCTGGGGGCCCTTGGGTGGTCTGGCTCGGAGCCCATCTGCACACTCTCTGGGATCCGA CCCTGATGATTACGCCAGCAGCGGCAGCAGCCTGGGTGGGTGAGACTCGCCTGTCTTTGAGGC CGGGGTGTTTGGGCTCCTCAGCCCCCTGCACCCCAAGGCGTCTTCCATCTTCAATCGCATC TCTGTCTCTGAGggaagcggagctactaacttcagcctgctgaagcaggctggagacgtggaggagaacctggagcctgtagcAT GGTGAGCAAGGGCGAGGAGCTGTTACCGGGGTGGTGCCCATCCTGGTCTGAGCTGGACGGCG ACGTAAACGGCCACAAGTTCAGCGTGTCCGGCGAGGGCGAGGGCGATGCCACCTACGGCAAGC TGACCTGGAAGTTCATCTGCACCAACGGCAAGCTGCCCTGGCCACCTCGTGACCCAC CCTGACCTACGGCGTGCAGTGCTTCAGCCGCTACCCCGACCACATGAAGCAGCAGCACTTCTTC AAGTCCGCCATGCCGAAGGCTACGTCCAGGAGCGCACCATCTTCTCAAGGACGACGGCAACT ACAAGACCCGCGCCGAGGTGAAGTTCAGAGGGCGACACCCTGGTGAACCGCATCGAGCTGAAGG GCATCGACTTCAAGGAGGACGGCAACATCCTGGGGCACAAGCTGGAGTACAACATAACAGCCA CAACGTCTATATCATGGCCGACAAGCAGAAGAAGGCATCAAGGTGAAGTTCAGATCCGCCAC AACATCGAGGACGGCAGCGTGCAGCTCGCCGACCACTACCAGCAGAACACCCCATCGCGGAC GGCCCCGTGCTGCTGCCGACAACCACTACCTGAGCACCCAGTCCGCCCTGAGCAAAGACCCC AACGAGAAGCGCGATCACATGGTCTGCTGGAGTTCGTGACCGCCGCGGGGATCACTCTCGGC ATGGACGAGCTGTACAAGTAA	GSG_P2A_AS is highlighted by underlining.
Zfp36-p2A-EGFP	ATGGCCATTGCGGCCACCATGGATCTCTCTGCCATCTACGAGAGCCTTATGTGATGAGCCATG ACCTGTACACCCGACCACGGAGGAAGTGAAGTCTCCGAGGACTTTGGAACATAAACTCATCGGA CTCCATCCCATCTGGGGTACCTCTCGCCTGACTGGCCGCTCCACTAGCCTGGTGGAGGGCCG AAGCTGCAGCTGGGTACCCCAACCCCTGGTTTCGACCCCTTGCTCCCCGCCGGGCCCTGA GCTGTACCCCTACCTACTTCGCCTACTGCAACTCCACCACCTCCTCTCGATACAAGACTGAGC TCTGTGCGACCTACTCAGAGAGCGGGCGTTGTGCTATGGGGCCAAGTGCCAGTTTGCCACAG GCCCGGGTGAAGTGCGCCAAGCCAATCGCCACCCCAAGTACAAAACGGAACTCTGCCACAAGTT CTACCTCAAGGGCCGCTGCCCTACGGCTCTCGATGCCACTTCATCCACAACCTTACCGAGGAC CTGGCTCTCCCTGGCCAGCCCCATGTGCTCCGACAAAGCATCAGCTTCTCAGGCTTGCCCTCAG GCCGAGAACCTCACCACACCTCCAGGCTTCTCTGGCCCTTCCCTGTCTCTTGTCTCTTTTCG CCTTCAGCTCCCCACCACCGCTGGGGACCTTCCACTTTCCCTTCTGCTTCTCTGCTGCC CTGGGACCCCTGTGTCTCGAAGAGACCTACCCAGCCTGTTGTCCCTCCTGCCGAAGGTCTAC TACCCCTAGCACCATCTGGGGGCCCTTGGGTGGTCTGGCTCGGAGCCCATCTGCACACTCTCTG GGATCCGACCCCTGATGATTACGCCAGCAGCGGCAGCAGCCTGGGTGGGTGAGCTCGCCTGTC TTTGAGGCCGGGGTGTGGGGCTCCTCAGCCCCCTGCACCCCAAGGCGTCTTCCATCTTCA ATCGCATCTCTGTCTCTGAGggaagcggagctactaacttcagcctgctgaagcaggctggagacgtggaggagaacctgga cctgtagcATGGTGAGCAAGGGCGAGGAGCTGTTACCGGGGTGGTGCCCATCCTGGTTCGAGCTG GACGCGACGTAACCGGCCACAAGTTCAGCGTGTCCGGCGAGGGCGAGGGCGATGCCACCTAC GGCAAGCTGACCCTGAAGTTTCTGTCACCAACCGGCAAGCTGCCCGTGCCCTGGCCACCCCTC GTGACCAACCTGACCTACGGCGTGCAGTGCTTCAGCCGCTACCCGACCACATGAAGCAGAC GACTTCTTCAAGTCCGCCATGCCGAAGGCTACGTCCAGGAGCGCACCATCTTCTTCAAGGACG ACGGCAACTACAAGACCCGCGCCGAGGTGAAGTTCGAGGGCGACACCCTGGTGAACCGCATCG AGTGGAAGGGCATCGACTTCAAGGAGGACGGCAACATCCTGGGGCACAAGCTGGAGTACAACATA CAACAGCCACAACGTCTATATCATGGCCGACAAGCAGAAGAAGCGCATCAAGGTGAAGTTCAG ATCCGCCACAACATCGAGGACGGCAGCGTGCAGCTCGCCGACCACTACCAGCAGAACACCCCTC ATCGGCGACGGCCCCGTGCTGCTGCCGACAACCACTACCTGAGCACCCAGTCCGCCCTGAGC AAAGACCCCAACGAGAAGCGCGATCACATGGTCTGCTGGAGTTCGTGACCGCCGCGGGGATC ACTCTCGCATGGACGAGCTGTACAAGTAA	GSG_P2A_AS is highlighted by underlining.